J Solid State Electrochem (2010) 14:1761–1767
DOI 10.1007/s10008-010-1098-5

ORIGINAL PAPER

Development of sulfide glass-ceramic electrolytes for all-solid-state lithium rechargeable batteries

Akitoshi Hayashi · Keiichi Minami · Masahiro Tatsumisago

Received: 18 November 2009 / Revised: 30 April 2010 / Accepted: 10 May 2010 / Published online: 26 May 2010

Abstract Development of Li_2S–P_2S_5-based glass-ceramic electrolytes is reviewed. Superionic crystals of $Li_7P_3S_{11}$ and $Li_{3.25}P_{0.95}S_4$ were precipitated from the Li_2S–P_2S_5 glasses at the selected compositions. These high temperature or metastable phases enhanced conductivity of glass ceramics up to over 10^{-3} S cm^{-1} at room temperature. The original (or mother) glass electrolytes itself showed somewhat lower conductivity of 10^{-4} S cm^{-1} and have important role as a precursor for obtaining the superionic crystals, which were not synthesized by a conventional solid-state reaction. The substitution of P_2O_5 for P_2S_5 at the composition $70Li_2S{\cdot}30P_2S_5$ (mol%) improved both conductivity and electrochemical stability of glass-ceramic electrolytes. The all-solid-state In/$LiCoO_2$ cell using the $70Li_2S{\cdot}27P_2S_5{\cdot}3P_2O_5$ (mol%) glass-ceramic electrolyte showed initial capacity of 105 mAh g^{-1} (gram of $LiCoO_2$) at the current density of 0.13 mA cm^{-2} and exhibited higher electrochemical performance than that using the $70Li_2S{\cdot}30P_2S_5$ glass-ceramic electrolyte.

Keywords Solid electrolyte · Glass · Glass ceramic · Sulfide · Lithium battery · All-solid-state battery

Introduction

All-solid-state lithium rechargeable batteries have attracted much attention because the replacement of conventional liquid electrolytes with inorganic solid electrolytes essentially improves safety and reliability of lithium batteries [1–4]. There are two approaches of developing all-solid-state batteries: one is a thin film micro battery prepared by RF sputtering and laser ablation and the other is a bulk-type battery constructed of electrolyte and electrode powders. Several all-solid-state thin film batteries with the lithium phosphorus oxynitride (LiPON) glass as an electrolyte were reported to show excellent long-cycling performances at room temperature. The ambient conductivity of the LiPON is about 10^{-6} S cm^{-1}, which is not so high in lithium ion conductors reported so far. The LiPON can be applied as a solid electrolyte to thin film batteries because total resistance of electrolyte is kept small by reducing the thickness of the electrolyte film. The bulk-type battery has an advantage of enhancing cell capacity by the addition of large amounts of active materials to the cell. Utilizing highly lithium ion conducting solid electrolytes is a key to improve the cell performance.

Lithium ion conducting solid electrolytes have been extensively developed during the last three decades. The inorganic solid electrolytes offer advantages over liquid and organic polymer electrolytes such as free of hazards of leakage and nonflammability. Single ion conduction is also an important feature of inorganic materials. Only Li ions are mobile while the counter anions and other cations form a rigid network, suggesting that undesirable side reactions or decomposition of the electrolytes due to anion conduction would be suppressed in electrochemical cells.

In general, sulfide electrolytes are known to show higher conductivity than oxide electrolytes. Li_2S-based glasses [5–7] and crystals [8, 9] exhibited lithium ion conductivity of 10^{-4}–10^{-3} S cm^{-1} at room temperature. Sulfide glass ceramics, which are prepared by crystallization of sulfide glasses, are also attractive solid electrolytes. In particular, the glass ceramics in the binary system Li_2S–P_2S_5 showed

A. Hayashi (✉) · K. Minami · M. Tatsumisago
Department of Applied Chemistry, Osaka Prefecture University,
1-1 Gakuen-cho, Naka-ku, Sakai,
Osaka 599-8531, Japan
e-mail: hayashi@chem.osakafu-u.ac.jp

high conductivity of over 10^{-3} S cm^{-1} because superionic crystalline phases were precipitated by careful heat treatment of mother glasses [10–12]. Those superionic crystals are mostly metastable or high-temperature phases, which are difficult to be synthesized by conventional solid-state reaction.

In this paper, the development of Li_2S–P_2S_5-based glass-ceramic electrolytes is reviewed. The mechanical milling and melt quenching methods were used for preparation of the Li_2S–P_2S_5 glasses. The Li_2S–P_2S_5 glass ceramics were obtained by crystallization at several heat treatment temperatures from the glasses at different Li_2S compositions. Electrical and electrochemical properties and structure of the glass-ceramic electrolytes are demonstrated. Effects of the substitution of P_2O_5 for P_2S_5 on property and structure of Li_2S–P_2S_5 glass ceramics are discussed. The application of the Li_2S–P_2S_5–P_2O_5 glass-ceramic electrolytes to all-solid-state lithium rechargeable batteries is also reported.

Experimental

The glasses in the systems Li_2S–P_2S_5 and Li_2S–P_2S_5–P_2O_5 were prepared by mechanical milling using a planetary ball mill apparatus. The mixture of reagent-grade crystals of Li_2S (Idemitsu Kosan, 99.9%), P_2S_5 (Aldrich, 99%), and P_2O_5 (Aldrich, 99.99%) was put into an alumina pot with several alumina balls. The ball-milling process was conducted at room temperature under dry Ar atmosphere and the rotation speed was fixed to 370 rpm [13]. The glasses were also prepared by melt quenching. The mixture of reagent-grade crystals was put into a carbon-coated quartz tube and then the tube was sealed under vacuum. Melting condition was fixed at 750 °C for 10 h [14]. The glasses were obtained by quenching of molten samples with an ice water. The glass ceramics were prepared by heating the glasses at temperatures higher than the crystallization temperature. All the processes were carried out in a dry Ar-filled glove box.

X-ray diffraction measurements (CuKα) were performed using a diffractometer (M18XHF^{22}-SRA, MAC Science) to identify crystals in glass ceramics. Local structures of the samples were analyzed by Raman spectroscopy using a spectrometer (NR-1000, JASCO) equipped with an Ar^+ laser (514.5 nm) and solid-state ^{31}P MAS-NMR measurements using a spectrometer (Varian, Unity Inova 300). A single pulse sequence with $\pi/2$ pulse of 2.0 μs and a cycle pulse delay of 5.0 s were used in the NMR measurement. The size of electrolyte powders was examined by using a scanning electron microscope (SEM; JEOL, JSM-5300).

Electrical conductivities were measured for the pelletized samples with 10 mm in diameter and about 1 mm in thickness. A carbon paste diluted with anhydrous toluene was applied on both sides of a sample and carbon electrodes were formed after heat treatment. AC impedance measurements were carried out in dry Ar atmosphere using an impedance analyzer (SI1260, Solartron) in the frequency range of 10 Hz to 8 MHz.

Electrochemical properties of the glass ceramics were evaluated by a cyclic voltammetry technique. A stainless steel disk as a working electrode and a lithium foil as a counter electrode were attached on each face of the pellet. The potential sweep was performed using a potentiostat/galvanostat device (SI 1287, Solartron) with a scanning rate of 1 mV s^{-1}.

All-solid-state In/$LiCoO_2$ cells using the Li_2S–P_2S_5–P_2O_5 glass-ceramic electrolytes were constructed as follows. The $LiCoO_2$ (Toda Kogyo Corp.) and the glass-ceramic electrolyte with a weight ratio of 70:30 were mixed using an agate mortar to prepare a composite positive electrode. An indium foil was used as a negative electrode because indium electrode stably works as a counter electrode in all-solid-state cells using sulfide solid electrolytes [15]. A bilayer pellet consisting of the composite positive electrode (10 mg) and glass-ceramic solid electrolytes (80 mg) was obtained by pressing under 360 MPa(10 mmϕ); then indium foil was attached to the bilayer pellet by pressing under 240 MPa. The pellet was sandwiched in between two stainless steel rods; the stainless steel rods were used as current collectors for both positive and negative electrodes. All processes were performed in a dry Ar-filled glove box.

Results and discussion

Characterization of Li_2S–P_2S_5 glass electrolytes prepared by mechanical milling

The sulfide glasses in the binary system Li_2S–P_2S_5 were prepared by mechanical milling technique. The mechanochemical process is basically a room temperature process with no vaporization of sulfides. Fine powder electrolytes are obtained directly from starting materials by the process. Those fine sulfide electrolyte powders are suitable for good contact with the electrode materials in fabrication of bulk-type all-solid-state batteries. Figure 1 shows the SEM image of the $70Li_2S{\cdot}30P_2S_5$ (mol%) glass sample prepared by mechanical milling for 20 h. The obtained sample was agglomerated particles and the size of secondary particles was 1–5 μm. The sample showed halo pattern in X-ray diffraction and typical glass transition phenomenon at ca. 210 °C in thermal analysis, indicating that the obtained sample was in glass state.

Local structure of the milled glass was compared with that of glass prepared by conventional melt quenching.

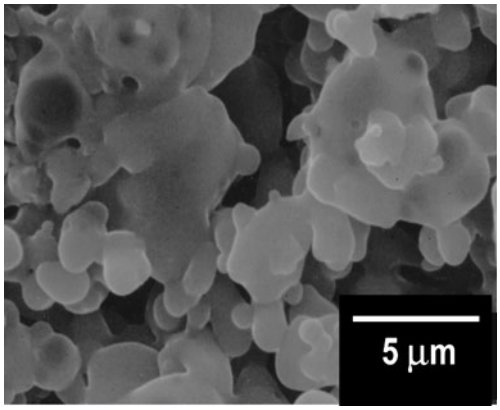

Fig. 1 SEM image of the $70Li_2S{\cdot}30P_2S_5$ (mol%) glass powder prepared by mechanical milling for 20 h

Figure 2 shows the Raman spectra of the $70Li_2S{\cdot}30P_2S_5$ glasses prepared by mechanical milling and melt quenching. The spectrum of the milled glass was quite similar to that of the quenched glass. Two peaks at 420 and 410 cm^{-1} were observed in both the spectra. The peaks at 420 and 410 cm^{-1} are attributable to the PS_4^{3-} and $P_2S_7^{4-}$ ions, respectively [16]. The local structure around phosphorus atoms of the milled glass was almost the same as that of the melt quenched glass.

Characterization of Li_2S–P_2S_5 glass-ceramic electrolytes

X-ray diffraction and differential thermal analysis were carried out for $xLi_2S(100-x)P_2S_5$ glass samples in the composition range from x=67 to 87.5 mol% prepared by mechanical milling for 20 h. Halo patterns were observed for all the glasses, although broad diffraction peaks due to the Li_2S crystal as a starting material were still present in the compositions with 80 mol% Li_2S or more. Furthermore, the first exothermic peak due to crystallization was observed in the temperature range from 220°C to 260°C for all the glasses. Hence, the Li_2S–P_2S_5 glass ceramics were prepared by heating the milled glasses over the first crystallization temperatures.

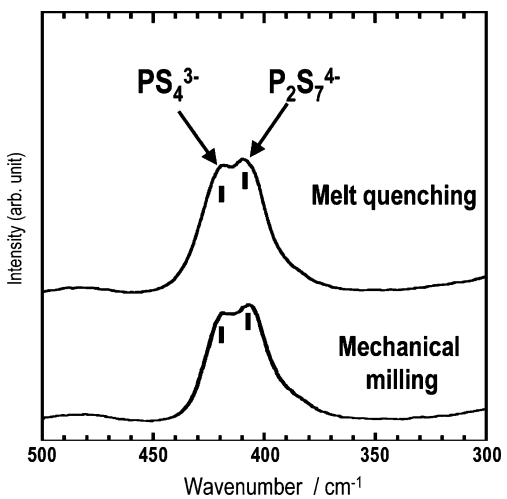

Fig. 2 Raman spectra of the $70Li_2S{\cdot}30P_2S_5$ (mol%) glasses prepared by mechanical milling and melt quenching

Figure 3 shows the XRD patterns of the $xLi_2S(100-x)P_2S_5$ (x=67, 70, 75, 80, and 87.5 mol%) glass ceramics. The $Li_4P_2S_6$ crystal was mainly precipitated in the glass ceramic with 67 mol% Li_2S, while the $Li_7P_3S_{11}$ crystal [17] was formed in the glass ceramic with 70 mol% Li_2S. In the glass ceramics with 75 mol% Li_2S or more, crystals analogous to thio-LISICON $Li_{3+x}Ge_xP_{1-x}S_4$ solid solution were precipitated. In the binary system Li_2S–P_2S_5 without any Ge atoms, $Li_{3+5y}P_{1-y}S_4$ with phosphorus deficiency would be formed; thio-LISICON region III ($Li_{3.2}Ge_{0.2}P_{0.8}S_4$) analog, the $Li_{3.2}P_{0.96}S_4$ crystal, was precipitated in the glass ceramic of x=75, while thio-LISICON region II ($Li_{3.25}Ge_{0.25}P_{0.75}S_4$) analog, the $Li_{3.25}P_{0.95}S_4$ crystal, was precipitated in the glass ceramics of x=80 and 87.5.

Crystals such as Li_3PS_4 and $Li_4P_2S_6$ showed low conductivity of below 10^{-7}S cm^{-1} at room temperature [16], resulting in lower conductivity of the glass ceramic of x=67. The thio-LISICON region II and III crystals were reported to show high conductivity of 2.2×10^{-3} and 6.4×10^{-4}S cm^{-1}, respectively [8]. The formation of highly conductive thio-LISICON analogs is responsible for the enhancement of conductivity (ca. 10^{-3}S cm^{-1}) by crystallization at the compositions with 75 mol% Li_2S or more.

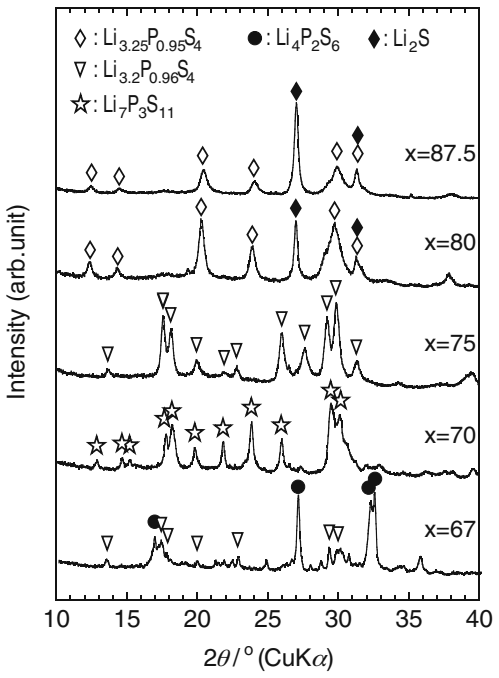

Fig. 3 XRD patterns of the $xLi_2S{\cdot}(100-x)P_2S_5$ (mol%) glass ceramics obtained by heating the glasses up to their first crystallization temperatures

Table 1 Crystalline phases, electrical conductivity at 25 °C, and activation energy for conduction of the $70Li_2S{\cdot}30P_2S_5$ (mol%) glass-ceramic electrolytes prepared by heat treatment at several temperatures

heat treatment temperature (°C)	Precipitated crystal	Conductivity at 25 °C (Scm^{-1})	Activation energy for conduction ($kJmol^{-1}$)
None	Glass	5.4×10^{-5}	38
250	$Li_7P_3S_{11}$	2.2×10^{-3}	18
360	$Li_7P_3S_{11}$	3.2×10^{-3}	12
550	$Li_4P_2S_6$, $Li_{3.2}P_{0.96}S_4$	1.1×10^{-6}	50
Solid-state reaction	$Li_4P_2S_6$, Li_3PS_4	1.0×10^{-8}	55

The data for the $70Li_2S{\cdot}30P_2S_5$ crystal prepared by solid-state reaction is also listed

The glass ceramic of $x=70$ with $Li_7P_3S_{11}$ showed the highest conductivity of 2.2×10^{-3} S cm^{-1} at room temperature and the lowest activation energy for conduction of 18 kJ mol^{-1} among all the Li_2S–P_2S_5 glass ceramics. The crystal structure of $Li_7P_3S_{11}$ was clarified by the Rietveld analysis based on synchrotron XRD measurements [17]. The compound crystallized in a triclinic cell with space group of *P*-1, and contains P_2S_7 ditetrahedra and PS_4 tetrahedra. The lithium atoms are located around the P_2S_7 and PS_4 and surrounded by three to five sulfur atoms.

The thermal stability of the superionic $Li_7P_3S_{11}$ crystal precipitated from the $70Li_2S{\cdot}30P_2S_5$ glass was investigated. Crystalline phases, electrical conductivity at 25 °C, and activation energy for conduction of the $70Li_2S{\cdot}30P_2S_5$ glass-ceramic electrolytes prepared by heat treatment at several temperatures are listed in Table 1. The data for the $70Li_2S{\cdot}30P_2S_5$ crystal prepared by solid-state reaction is also listed.

In the $70Li_2S{\cdot}30P_2S_5$ glass ceramic, the $Li_7P_3S_{11}$ crystal was precipitated as a primary crystal by heating the glass at 250 °C over the first crystallization temperature. The $Li_7P_3S_{11}$ crystal with higher crystallinity was present at heat treatment of 360 °C. The crystal, however, disappeared after heating up to 550 °C, and the $Li_4P_2S_6$ (main phase) and $Li_{3.2}P_{0.96}S_4$ crystals were formed; the $Li_4P_2S_6$ crystal was synthesized by solid-state reaction of Li_2S and P_2S_5 crystals. With an increase in heat treatment temperatures up to 550 °C, the $Li_7P_3S_{11}$ crystal was transformed to thermodynamically stable phases such as the $Li_4P_2S_6$ crystal. The $Li_7P_3S_{11}$ crystal was not synthesized by conventional solid-state reaction. Very recently, we have found that the $Li_7P_3S_{11}$ crystal was prepared from the $70Li_2S{\cdot}30P_2S_5$ melt [18]. The melt, which was obtained by heating at 750 °C for 10 h in a silica ampoule, was kept at 700 °C for 48 h for nucleation and crystal growth, and then quenched to room temperature. The $Li_7P_3S_{11}$ crystal was obtained as a single phase. The results above mentioned indicate that the $Li_7P_3S_{11}$ crystal is a high-temperature phase in the binary system Li_2S–P_2S_5. The glass electrolyte has an advantage as a precursor for stabilizing of a high-temperature phase of $Li_7P_3S_{11}$ at room temperature.

The relationship between precipitated crystals and conductive properties of the $70Li_2S{\cdot}30P_2S_5$ glass-ceramic electrolytes is discussed. The conductivity of the glass was 5.4×10^{-5} S cm^{-1} at 25 °C. The conductivities of the glass ceramics increased with increasing heat treatment temperature, and then the highest conductivity of 3.2×10^{-3} S cm^{-1} was observed after heating at 360 °C. The conductivity of the glass ceramic heated at 550 °C decreased to 1.1×10^{-6} S cm^{-1}. The heat treatment temperature dependence of the activation energies of the glass ceramics corresponded to that of the conductivities at 25 °C. The minimum activation energy of 12 kJ mol^{-1} was obtained for the glass ceramic heated at 360 °C; the activation energy is the lowest one in all the lithium ion conductors reported so far. The activation energy of the glass ceramic heated at 550 °C increased to 50 kJ mol^{-1}. The conductivities and activation energies of the $70Li_2S{\cdot}30P_2S_5$ glass ceramic largely depended on the precipitated crystalline phases. The formation of $Li_7P_3S_{11}$ brought about a remarkable enhancement on conducting properties. The crystallinity of $Li_7P_3S_{11}$ phase was increased by increasing heat treatment temperature from 250 °C to 360 °C, and this is responsible for the higher conductivity and lower activation energy of the glass

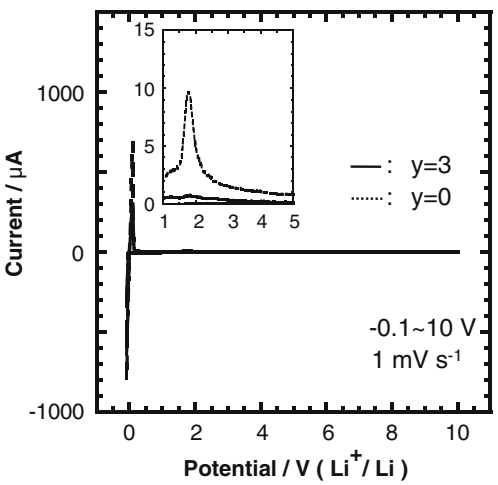

Fig. 4 Cyclic voltammograms of the $70Li_2S{\cdot}(30-y)P_2S_5{\cdot}yP_2O_5$ (y=0 and 3 mol%) glass-ceramic electrolytes

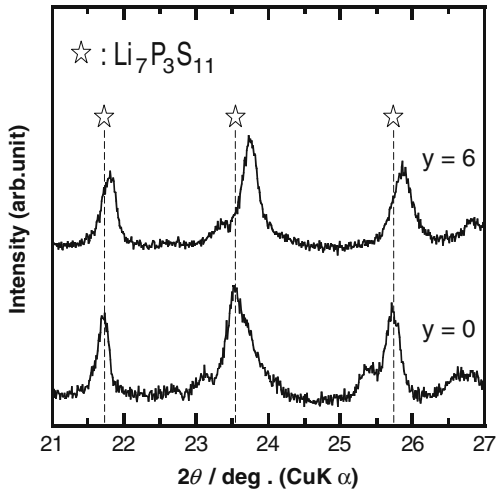

Fig. 5 XRD patterns of the $70Li_2S{\cdot}(30-y)P_2S_5{\cdot}yP_2O_5$ (y=0 and 6 mol%) glass ceramics in the limited angle range of $21°\leqq 2\theta \leqq 27°$

ceramic prepared at 360 °C. On the other hand, the precipitation of thermodynamically stable crystals such as $Li_4P_2S_6$ decreased the conductivity because the crystals consisted of $Li_4P_2S_6$ and Li_3PS_4 synthesized by solid-state reaction showed low conductivity of 1.0×10^{-8} S cm^{-1} and large activation energy of 55 kJ mol^{-1}. Hence, the formation of the high-temperature phase $Li_7P_3S_{11}$ is a key to achieve excellent conducting properties of the $70Li_2S{\cdot}30P_2S_5$ glass-ceramic electrolyte.

Characterization of Li_2S–P_2S_5–P_2O_5 glass-ceramic electrolytes

To improve properties of glass-ceramic electrolytes, a third component P_2O_5 was introduced to the Li_2S–P_2S_5 binary system. The effects of substituting P_2O_5 for P_2S_5 on properties and structure of glass ceramics were examined. The mother glasses in the system Li_2S–P_2S_5–P_2O_5 were prepared by melt quenching and mechanical milling. Here, we focus on the $70Li_2S{\cdot}(30-y)P_2S_5{\cdot}yP_2O_5$ (mol%) oxysulfide glasses prepared by melt quenching because the glass ceramic with 70 mol% Li_2S exhibited the highest conductivity in the Li_2S–P_2S_5 binary system as mentioned above.

The $70Li_2S{\cdot}(30-y)P_2S_5{\cdot}yP_2O_5$ oxysulfide glasses were heated at their first crystallization temperatures (ca. 280 °C) to form glass ceramics. Electrochemical stability of the glass ceramics as a solid electrolyte was investigated by cyclic voltammetry. Figure 4 shows the cyclic voltammograms of the $70Li_2S{\cdot}(30-y)P_2S_5{\cdot}yP_2O_5$ (y=0 and 3) glass ceramics at the first cycle in the potential range from −0.1 to 10 V (vs. Li^+/Li). The measurement was carried out at the scan speed of 1 mV s^{-1} at 25 °C. Current at the vertical axis was magnified in the potential range from 1 to 5 V and shown as an inset figure. Both cathodic and anodic current peaks attributable to deposition/dissolution of lithium metal were observed in the potential range from −0.1 to +0.3 V, suggesting that both the glass-ceramic electrolytes are electrochemically stable for lithium metal. The glass ceramics basically exhibited a wide electrochemical window of ca. 10 V because no large anodic current was observed up to 10 V. However, a very small anodic current (ca. 10 μA) compared to the current of the lithium deposition/dissolution reaction (ca. 800 μA) appeared at the voltage ca. 2 V for the $70Li_2S{\cdot}30P_2S_5$ glass ceramic (x= 0). On the other hand, no obvious anodic current at 2 V was observed for the $70Li_2S{\cdot}27P_2S_5{\cdot}3P_2O_5$ glass ceramic (y=3). Substitution of 3 mol% of P_2O_5 for P_2S_5 is useful for improving electrochemical stability of the glass ceramics. The small anodic peak at ca. 2 V is probably attributable to the oxidation of S^{2-} free ions as a similar behavior was

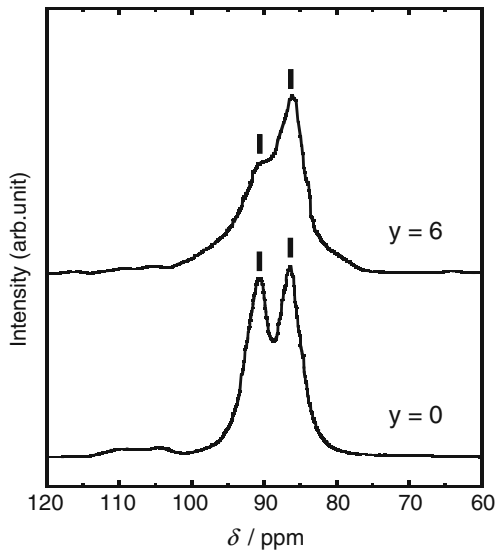

Fig. 6 ^{31}P MAS-NMR spectra of the $70Li_2S{\cdot}(30-y)P_2S_5{\cdot}yP_2O_5$ (y=0 and 6 mol%) glasses ceramics

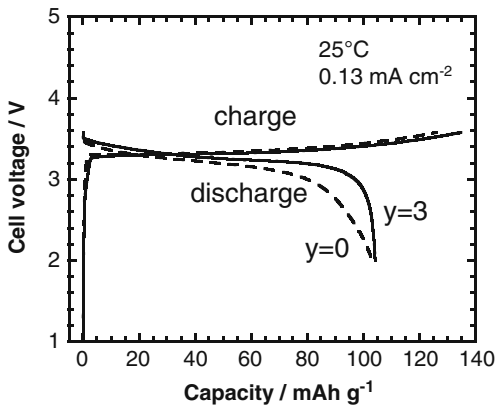

Fig. 7 Initial charge–discharge curves for all-solid-state In/$LiCoO_2$ cells using the $70Li_2S{\cdot}(30-y)P_2S_5{\cdot}yP_2O_5$ (y=0 and 3 mol%) glass-ceramic electrolytes

observed in the cyclic voltammogram of the $67Li_2S{\cdot}33P_2S_5$ glass [19].

Electrical conductivity of glass ceramics was also increased by the substitution of small amounts of P_2O_5. The glass ceramic with 3 mol% P_2O_5 exhibited the conductivity of 3.0×10^{-3} S cm^{-1} at room temperature, which is higher than that of the $70Li_2S{\cdot}30P_2S_5$ glass ceramic without substitution [20]. The activation energy for conduction of $70Li_2S{\cdot}27P_2S_5{\cdot}3P_2O_5$ glass ceramic was 16 kJ mol^{-1} and the value is the minimum at all the compositions $70Li_2S{\cdot}(30-y)P_2S_5{\cdot}yP_2O_5$.

XRD patterns attributable to $Li_7P_3S_{11}$ were basically observed for the $70Li_2S{\cdot}(30-y)P_2S_5{\cdot}yP_2O_5$ glass ceramics as shown in Fig. 5. In detail, the diffraction peaks due to $Li_7P_3S_{11}$ shifted to the higher diffraction angle side for the glass ceramics with 6 mol% P_2O_5, suggesting that the oxygen atoms were incorporated into the $Li_7P_3S_{11}$ crystal. Figure 6 shows the ^{31}P MAS-NMR spectra of the glass ceramics at the compositions of $70Li_2S{\cdot}(30-y)P_2S_5{\cdot}yP_2O_5$ (y=0 and 6). The peaks at 86 and 91 ppm are attributable to the (PS_4+POS_3) structural unit and the P_2S_7 unit, respectively [20]. The intensity of the peak due to the P_2S_7 unit was decreased with an increase in P_2O_5 content while that due to the (PS_4+POS_3) unit was increased. It was suggested that the P_2OS_6 oxysulfide unit, where a bridging oxygen is substituted for a bridging sulfur in the P_2S_7 unit, would be partially formed in the $70Li_2S{\cdot}24P_2S_5{\cdot}6P_2O_5$ glass ceramic. The structural analyses mentioned above suggest that an oxygen-incorporated $Li_7P_3S_{11}$ crystal ($Li_7P_3S_{11-z}O_z$) was formed in the $70Li_2S{\cdot}(30-y)P_2S_5{\cdot}yP_2O_5$ glass ceramics. Electrical and electrochemical properties of glass ceramics mainly depend on the precipitated crystals. Those properties of the $70Li_2S{\cdot}30P_2S_5$ glass ceramic was improved by the partial substitution of P_2O_5, suggesting that the $Li_7P_3S_{11-z}O_z$ crystal would have higher conductivity and electrochemical stability than the $Li_7P_3S_{11}$ crystal without substitution.

All-solid-state In/$LiCoO_2$ cells using the $70Li_2S{\cdot}(30-y)P_2S_5{\cdot}yP_2O_5$ (x=0 and 3) glass-ceramic electrolytes were constructed. The glass ceramics were obtained by crystallization of the mother glasses prepared by mechanical milling. Figure 7 shows initial charge–discharge curves of all-solid-state In/$LiCoO_2$ cells. The cell capacity is shown as the capacity per gram of $LiCoO_2$. The measurements were carried out at the current density of 0.13 mA cm^{-2} in the voltage range from 2.0 to 3.6 V (vs. Li–In counter electrode), which corresponds to 2.6 to 4.2 V (vs. Li electrode). Both the cells were charged and then discharged at 25°C. Charge–discharge plateaux were somewhat different in both the cells; the cell using the $70Li_2S{\cdot}27P_2S_5{\cdot}3P_2O_5$ oxysulfide electrolyte showed slightly lower charge plateau and higher discharge plateau than the cell using the $70Li_2S{\cdot}30P_2S_5$ sulfide electrolyte. The electrochemical performance of the former cell was better than that of the latter cell, although both the cells exhibited almost the same discharge capacity of 105 mAh g^{-1}. The enhancement of electrochemical stability and conductivity in the oxysulfide solid electrolyte is a possible reason for improvement of electrochemical performance of all-solid-state cells.

Conclusions

Properties and structure of glass-ceramic electrolytes in the systems Li_2S–P_2S_5 and Li_2S–P_2S_5–P_2O_5 were investigated. The mother glasses for obtaining glass ceramics were prepared by mechanical milling as well as melt quenching. Superionic crystals of $Li_7P_3S_{11}$ and $Li_{3.25}P_{0.95}S_4$ were precipitated from the Li_2S–P_2S_5 glasses at the selected compositions, and these high temperature or metastable crystals enhanced conductivity of glass ceramics up to over 10^{-3} S cm^{-1} at room temperature. The glass electrolytes itself showed conductivity of 10^{-4} S cm^{-1} and have important role as a precursor for obtaining the superionic phases, which were not synthesized by a conventional solid-state reaction. The substitution of P_2O_5 for P_2S_5 at the composition $70Li_2S{\cdot}30P_2S_5$ improved both conductivity and electrochemical stability. The all-solid-state In/$LiCoO_2$ cell using the $70Li_2S{\cdot}27P_2S_5{\cdot}3P_2O_5$ glass-ceramic electrolyte exhibited better electrochemical performance than that using the $70Li_2S{\cdot}30P_2S_5$ glass-ceramic electrolyte. The formation of an effective interface between active material and solid electrolyte would improve battery performance. The coating of active material with oxide thin films was reported to be useful for decreasing interfacial resistance and enhancing rate performance of all-solid-state cells [21, 22]. Further development of solid electrolyte itself and interfacial design is needed for realizing all-solid-state cells with higher energy density and higher power density.

Acknowledgment This work was supported by a Grant-in-Aid for Scientific Research from the Ministry of Education, Culture, Sports, Science and Technology of Japan and also supported by the New Energy and Industrial Technology Development Organization (NEDO) of Japan.

References

1. Minami T, Tatsumisago M, Wakihara M, Iwakura C, Kohjiya S, Tanaka I (2005) Solid state ionics for batteries. Springer-Verlag, Tokyo
2. Bates JB, Dudney NJ, Neudecker B, Ueda A, Evans CD (2000) Solid State Ion 135:33
3. Iwamoto K, Aotani N, Takada K, Kondo S (1995) Solid State Ion 79:288

4. Komiya R, Hayashi A, Morimoto H, Tatsumisago M, Minami T (2001) Solid State Ion 140:83
5. Mercier R, Malugani JP, Fahys B, Robert G (1981) Solid State Ion 5:663
6. Pradel A, Ribes M (1986) Solid State Ion 18–19:351
7. Tatsumisago M, Hirai K, Minami T, Takada K, Kondo S (1993) J Ceram Soc Jpn 101:1315
8. Kanno R, Murayama M (2001) J Electrochem Soc 148:742
9. Murayama M, Sonoyama N, Yamada A, Kanno R (2004) Solid State Ion 170:173
10. Hayashi A, Hama S, Minami T, Tatsumisago M (2003) Electrochem Commun 5:111
11. Mizuno F, Hayashi A, Tadanaga K, Tatsumisago M (2005) Adv Mater 17:918
12. Mizuno F, Hayashi A, Tadanaga K, Tatsumisago M (2006) Solid State Ion 177:2721
13. Hayashi A, Hama S, Morimoto H, Tatsumisago M, Minami T (2001) J Am Ceram Soc 84:477
14. Minami K, Mizuno F, Hayashi A, Tatsumisago M (2007) Solid State Ion 178:837
15. Takada K, Aotani N, Iwamoto K, Kondo S (1996) Solid State Ion 136–137:877
16. Tachez M, Malugani P, Mercier R, Robert G (1984) Solid State Ion 14:181
17. Yamane H, Shibata M, Shimane Y, Junke T, Seino Y, Adams S, Minami K, Hayashi A, Tatsumisago M (2007) Solid State Ion 178:1163
18. Minami K, Hayashi A, Tatsumisago M (2010) J Ceram Soc Jpn 118:305
19. Machida N, Yamamoto H, Shigematsu T (2004) Chem Lett 33:30
20. Minami K, Mizuno F, Hayashi A, Tatsumisago M (2008) J Non-Cryst Solids 354:370
21. Ohta N, Takada K, Zhang L, Ma R, Osada M, Sasaki T (2006) Adv Mater 18:2226
22. Sakuda A, Kitaura H, Hayashi A, Tadanaga K, Tatsumisago M (2009) J Electrochem Soc 156:A27